AIAA SciTech
Guidance, Navigation & Control Conference
4-8 Jan 2016, San Diego, CA, USA

AIAA 2016-1136

Compound eye sensor for real-time aircraft wing deflection measurement

Susan A. Frost[1]
NASA Ames Research Center, Moffett Field, CA 94035

George E. Gorospe[2], Christopher Teubert [3]
SGT Inc., NASA Ames Research Center, Moffett Field, CA 94035

We report on an optical sensor based on the physiological aspects of the eye and vision-related neural layers of the common housefly (Musca domestica) that has been developed and built for aerospace applications. The intent of the research is to produce a position sensor with high functionality in low-light and low-contrast environments, high sensitivity to motion, and a compact size, which is lightweight, and has low power and computation requirements. The compound eye sensor uses a combination of overlapping photoreceptor responses that are well approximated by Gaussian distributions and neural superposition to detect image features, such as object motion, to a much higher degree than just the photoreceptor density would imply. The Gaussian overlap in the sensor comes from the front-end optical design, and the neural superposition is accomplished by subsequently combining the signals using analog electronics. The compound eye sensor is being developed to perform real-time tracking of a target on a flexible aircraft wing experiencing bending and torsion loads during flight. We report on results of laboratory experiments using the compound eye sensor to sense a target moving across its field of view.

I. Introduction

In an effort to reduce the environmental impact of aviation, lighter weight aircraft configurations are being considered [1]. One challenge of lightweight aircraft wings is increased flexibility that can adversely affect handling qualities and safety. Approaches using active control to mitigate problems associated with flexible wings have been proposed [2]-[6]. Knowledge of aircraft wing position during flight can provide significant advantages to the effectiveness of these approaches. Current approaches for measuring wing deflection, including strain measurement devices, accelerometers, or GPS solutions, and new technologies such as fiber optic strain sensors, have limitations for their practical application to flexible aircraft control. Traditional machine vision systems using charge coupled device (CCD) or complementary metal oxide semiconductor (CMOS) arrays have several disadvantages for applications requiring high sensitivity to motion and high speed extraction of certain image features such as the object edges of a target, including the blurring of objects moving at high speed, and the high computation and data throughput requirements for edge detection [7]-[8]. A machine vision system that can perform high speed target tracking in near real-time with low power requirements is desirable for wing deflection tracking.

An optical sensor originally inspired by the physiological aspects of the eye (and vision-related neural layers) of the common housefly (*Musca domestica*) is under development by researchers at NASA Ames Research Center. This development effort is building upon the work done as collaboration between researchers at the University of Wyoming [9-11] and NASA Ames Research Center. The intent of the early research was to design a sensor with high functionality in low-light and low-contrast environments, sensitivity to motion, compact size, and low power and computation requirements.

[1]Research Scientist, Intelligent Systems Division, M/S 269-3, AIAA Senior Member.
[2]Researcher, Intelligent Systems Division, M/S 269-3.
[3]Researcher, Intelligent Systems Division, M/S 269-3, AIAA Member.

The compound eye sensor uses a combination of quasi-Gaussian overlapping photoreceptor responses (see Fig. 1) and neural superposition to achieve what has been described in the literature as "hyperacuity," or the ability to detect image features, such as object motion, to a much higher degree than just the photoreceptor density would imply. The overlapping Gaussian response fields-of-view (FoVs) allow for very precise and fine measurements of position, direction, and speed.

Since the sensor excels in detection of even minute motion, a feasibility study using the sensor for detailed target tracking was proposed. The purpose is to track a known target pattern at relatively short range, and resolve the position and velocity of the pattern relative to a neutral position. One application is the precise measurement of wing deflection in a fixed wing aircraft. This optical approach allows for a faster, more efficient and accurate approach than alternative methods (such as accelerometers or strain gages within the target object). This method does have drawbacks however, such as its reliance on a clean line-of-sight to the target.

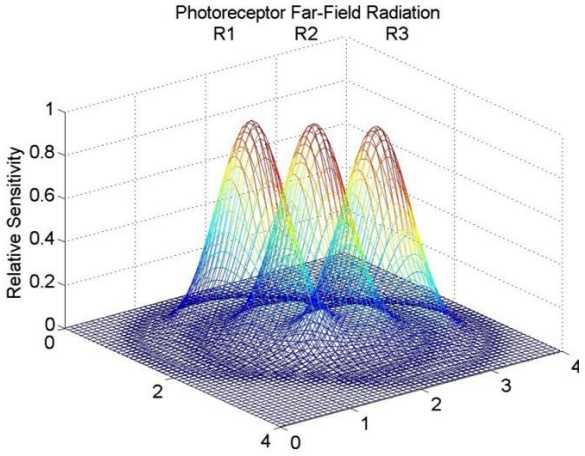

Fig. 1. Depiction of overlapping Gaussian response observed by the compound eye sensor

II. Sensor design and construction

The sensor platform consists of the sensor head and the sensor printed circuit board (PCB). The sensor head has seven photoreceptors that are connected to seven separate photodiodes located on the sensor PCB with seven equal length fiber optic cables. Each photodiode has its own channel on the PCB for current to voltage conversion followed by signal conditioning and filtering. This process occurs in parallel for each channel.

This section describes the function and composition of each subsystem within the compound eye sensor PCB as designed by Dean [9]. The subsystems are implemented as analog circuits. The sensor described here uses seven fiber-optically fed IFD91 photodarlington detectors [12]. These semiconductive devices output a current proportional to the number of photons impinging on the element (i.e. the quantity of light in front of the element). This current is small (on the order of 0.1 μA to 10 mA) and thus requires both conversion to a voltage as well as amplification. Following the photodarlingtons, a logarithmic compression amplifier circuit is used to achieve current-to-voltage conversion and to enable increased dynamic range of the output values. Use of the sensor in a wide variety of ambient lighting conditions, such as from dim light to extremely bright conditions, requires such increased dynamic range to ensure adequate image contrast for detection purposes.

Fig. 2. Front view of sensor head or "photoreceptor".

Two active filters are used to remove noise present in the signal. These filters include a 4th-order Butterworth low-pass filter with a 50 Hz cutoff frequency and a notch filter centered at 60 Hz. These filters specifically target noise sources that manifest themselves as flicker in interior lighting, which is well within the detection range of the sensor. Since the signal of interest is in the near-DC range, a low-pass filter is used. The outputs from this stage are considered the final sensor output signals, which can then be sampled.

Fig. 3. Detail of two photoreceptors in sensor head, where w represents the distance between the lens and the image plane and Δ φ represents the angle between two lenses.

The sensor (Fig. 2) has an optically optimized sensor head with a 12 mm outer diameter. The sensor head housing was designed to incorporate the multi-aperture nature of a compound eye. It was optimized with respect to response, motion acuity, and scalability. Results of the optimization suggested an ideal distance between the lens and the image plane of about w = 2.4 mm for pre-blurring, and an inter-lens angle of Δ φ = 7.5°, see Fig. 3. The housing holds seven lenses and seven optical fibers. The head is machine-milled aluminum, with 1 mm, multi-modal, single-fiber optical light guides connecting it to the circuit board. The 3 mm lenses focus the incoming light onto the image plane at the terminating ends of the light guides.

The sensor is calibrated by directing all facets toward an evenly lit, single-color, specular reflection free background. Then, using software, a running average for each channel is calculated. To calibrate Channels 2 through 6 their relative difference with respect to Channel 1 is added or subtracted from their original value. This results in all seven channels responding with an equal voltage to the calibration background. The response of each channel is scaled through a process in which a dark target traverses the full field of view of the sensor head providing equal input to each channel. This causes the voltage from each channel to fall as the target enters the field of view, reaching the minimum as it crosses the center of the field of view then rising again as it leaves the field of view. The response range of each channel is then computed, compared with Channel 1 and scaled to achieve an equivalent response range. In this way, scaling manages the filter out differences in performance between the individual photoreceptors, the photodiodes, and the signal processing channels. In an ideal lab setup, a curved Lambertian surface would be used to ensure that each of the seven channels is receiving stimulus that is not dependent on the viewing angle. This arrangement cannot be achieved with the facilities available, so the alternative approach was used. The maximum output voltage difference measured after calibration in the lab is approximately 10 millivolts.

A hyperacuity to motion is a compelling attribute of this sensor package. As a target moves within the sensor's FOV, the response is nearly immediate. The photodetectors measure the quantity of light within their range. For example, a target that is darker than the background causes a decrease in the output of a photodetectors sensing the target. Tracking multiple outputs at once allows for the determination of the direction and speed of such a target.

Table 1: Characterization parameters for sensor measured over numerous trails.

Parameter	Min	Typical	Max
Output [V]	~0.0	0.49	0.72
Operating Range [cm]		25.4	~130-150
Field of View		~40°	~42°
Sensor, PCB, and Cables Weight [g]		135	
Input Illuminance [lx]	1	520	36,000
Power Consumption [W]		3.3	

Characterization tests have indicated a number of operating parameters for the system (see Table 1). These describe general operating conditions for the sensor package. Extreme conditions may result in different behavior. The logarithmic compression system is designed to operate up to 72,000 luminance (or lux) [9], which, as Table 1 indicates, is far above the highest generated in the lab setting. For this sensor field of View (FOV) is defined as *the extent of the observable world that produces a* ***useful*** *response in the output of the compound eye sensor*. Useful in this case refers to the signal being usable for tracking. While the operating range between the sensor and the target indicated in Table 1 is sufficient for the demands of this project, augmented range may be realized for other applications by using additional optics in front of the sensor head.

III. Sensor Simulation

The Compound Eye Research and Simulation Package has been developed in MATLAB™ to aid with research activities. This program can simulate the sensor output for a moving target of arbitrary shape and size against a background. The target-background contrast can be varied, and the target movement can be controlled in front of the sensor. The simulation has the flexibility of simulating multiple sensors at various sensor-target distances and orientations with respect to the target. The assumption of paraxial theory of light is used to simulate the sensor response to the target-background combination. This assumption is found valid from the simulation results, because the simulation program incorporates only the total amount of light from the scene that is brought to focus on the tip of the fibers. Uniformity of the light intensity, and Lambertian reflectance throughout the surface of the background is also assumed. The output of the sensor is deemed ideal (disregarding the non-ideality due to higher order optical properties such as diffraction of the lenses). Also, noise with different distributions and power levels can be added to the simulated output to analyze the real world application scenario.

Figure 4 shows the experimental setup used for simulating a moving target on the target plane at a certain distance d from the virtual converging point of the sensor housing. The inter-lens angle $\Delta\varphi = 7.5°$ (see Fig. 2) comes from the optical front-end design. The angular roll off of an individual lens' response must decrease with the increase in object distance. This implies the spread of the Gaussian response must increase with the increase in sensor-target distance. The Gaussian depicting the sensor response (see Fig. 1) has a standard deviation (σ) of 7.5°. This was calculated using a ray-tracing optical simulation of the Compound Eye Photoreceptor and confirmed experimentally. The resulting sensitivities can be seen projected onto the background in Fig. 4. The simulation was validated using experimental data.

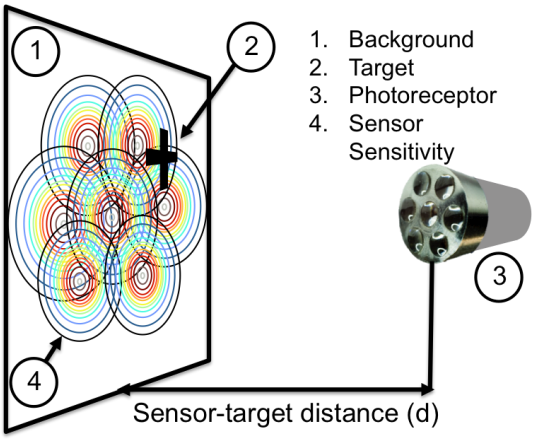

Fig. 4. Simulation experimental setup.

Fig. 5. Sensor orientation for simulation and hardware experiments. The numbers correspond to the sensor's diode numbers.

The sensor rotation relative to the target's movement direction is described with an additional parameter "sensor rotation", which is the angle between the horizontal axis, and the position of the optical element interfaced with photodiode D1 of Channel 1. The parameter "rotation" is introduced here to describe how much the sensor head has to be rotated for a particular application with respect to the horizontal axis (i.e., the axis parallel to the ground). Figure 5 shows the sensor orientation with a rotation of 0°, where 1 to 7 denote the positions of the seven photodiodes associated with the seven optical axes of the sensor. This arrangement is done to make the target movement vector parallel to the line passing through photoreceptors 1, 7, and 4, hereafter referred to as D1, D7, D4.

Figure 6 shows the results of a 5 mm wide target moving from outside of the sensor's FOV horizontally across the entire FOV. Note that as the target passes over the optical axis of a diode, the response from that diode reaches a lower limit. This is expected since the target is black against a white background, and so the number of photons reaching the photodiode are at the lowest level when the target is centered over the photodiode's FOV. Likewise, the response is greatest when the target is outside of a photodiode's FOV because the photoreceptor is only registering the white background.

A baseline tracking algorithm has been implemented to track the movement of a simple bar target. The algorithm makes use of difference signals between adjacent diodes. Differencing is used in the vision system of the housefly to determine edges. Figure 7 shows the signals and difference signals from the simulated target motion described above. Figure 8 shows the results of the tracking algorithm compared to the truth position.

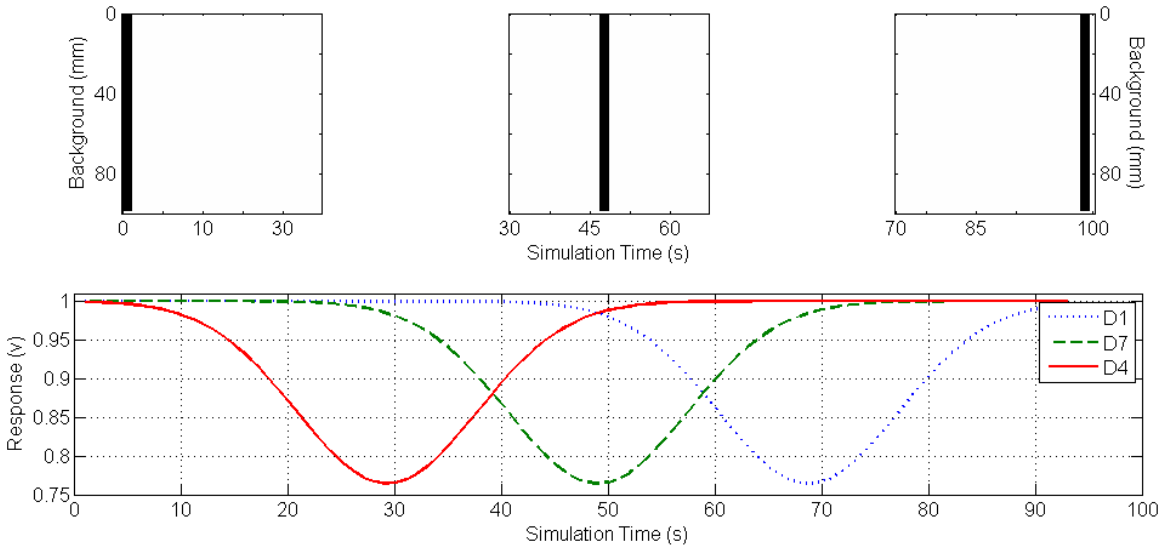

Fig. 6. Simulated target motion across the background (top). Signals from simulation with continuous target motion starting to the left of diode D4 and moving to the right until it crosses out of the FOV of diode D1 (bottom).

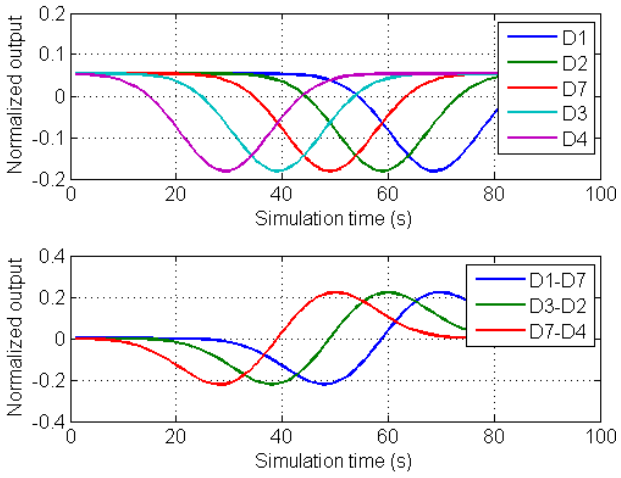

Figure 7. Simulation signals (top), difference signals (e.g., diode D1 – diode D7) (bottom).

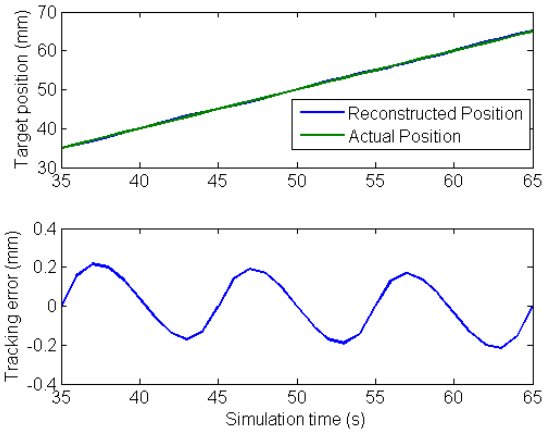

Figure 8. Reconstructed position (top) and tracking error (bottom).

IV. Sensor Testbed

A sensor demonstration testbed was designed and built at NASA Ames Research Center to test and characterize sensors, targets, and target tracking algorithm performance. The testbed includes a National Instruments (NI) SBC-68 chassis, the sensor signal processing board, and a light isolation box, which encloses the sensor head mount, the target positioning system, a LED based lighting system and CCD camera.

The sensor head mount, Fig. 9, allows the sensor to be precisely positioned relative to the target. The target position control system, Fig. 10, is controlled via a remote controller that can oscillate the target through horizontal translation up to 2.6 cm and axial rotation up to 10 degrees at frequencies up to 2 Hz. The LED based lighting system is used to produce a variety of lighting conditions with a circular array of LED pixels capable of red, green, and blue hues as well as 255 discrete brightness levels. The CCD camera, produced by Edmund Optics, is a 1.3 megapixel USB camera operating at 15 frames per second and produces the target position ground truth through a separate target-tracking algorithm.

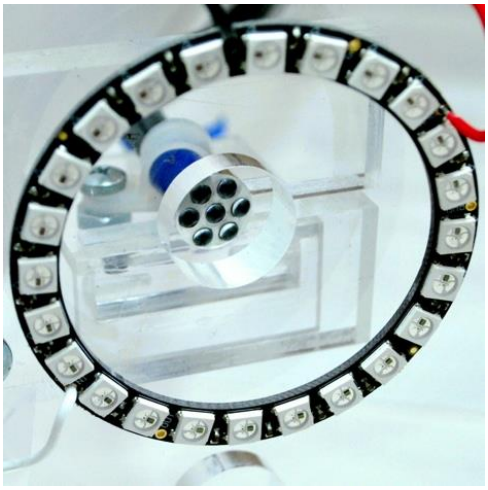

Fig. 9. Close up of the sensor head and LED array on the mount.

The light isolation box with a foam lip provides a region 42 cm x 93 cm x 62 cm for placement of the sensor and target. The box can be opened for modification of the test setup or shut to completely isolate the equipment from external light during experimentation. The inside walls of the light isolation box are a matte black surface. The sensor head mount, target positioning system, CCD camera, and light box are all mounted on a large optical bench, ensuring constant spatial positioning.

Outside the light isolation box, the sensor signal processing board produces voltages that are collected by a single NI SBC-68 chassis performing data acquisition. Data visualization occurs via a LabVIEW® interface.

The sensor development testbed provides a controlled environment for sensor benchmarking and experimentation. Experimental variables can include target distance from sensor, target motion and light levels in the environment.

V. Application Specification

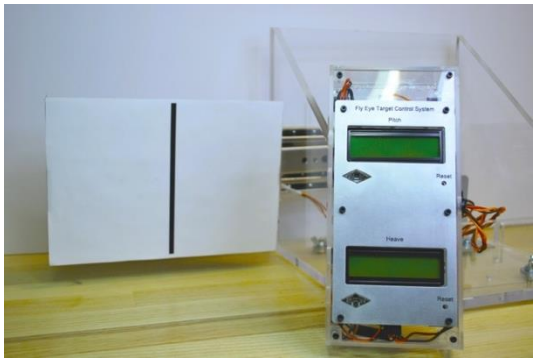

Fig. 10. The target position control system and remote controller.

A key requirement of the application proposed here is to measure the deflection of an aircraft wing from its resting position in real or near-real time. We consider a small Unmanned Aerial System (UAS), where the wing can bend a maximum of 3 cm from its resting position, with oscillation frequencies of less than 3 Hz. The sensor-target distance would be about 1 m, and the size of the target can be increased up to 25 cm in width. The height of the target can be increased up to the span of a wing (which is very large compared to the FOV of the sensor for this application). That is, we have some flexibility in determining the shape and size of the target, and the distance between the sensor and the target. The wing deflection may include bending and twist, but for this research twist is ignored. So, the key goal of this research is the real, or near-real, time tracking of a linearly moving target. A top-level diagram of the sensor-target arrangement is shown in Figure 11, where the sensor is mounted on the fuselage of the aircraft, and the target is painted on the surface of the wing. The sensor is looking down at the wing and out the wing. The out-of-plane bending motion of the wing is defined as when the wing bends in the direction up or down. Measuring the torsion or twist of the wing is a long-term goal of the project, but for now, the most important measure is the out-of-plane bending measured by one target on the wing.

Many researchers report on studies to estimate out-of-plane displacements by measuring in-plane strains. Using a cantilevered plate in the laboratory, Haugse et al. [13, 14] developed a modal transformation algorithm to recover deformations from strains. In a similar procedure, Pisoni and Santolini [15] determined the displacements at any given point in a vibrating clamped-end beam under different loading conditions using two strain gages. Li and Ulsoy [16] presented a method to measure tool-tip displacement of a precision line-boring machine. Davis et al. [17] and Kim et al. [18] measured vertical deflections of simple beam models using fiber Bragg grating (FBG) sensor signals. The key concept of these strain-based techniques is that the vibration displacement can be expressed in terms of an infinite number of vibration

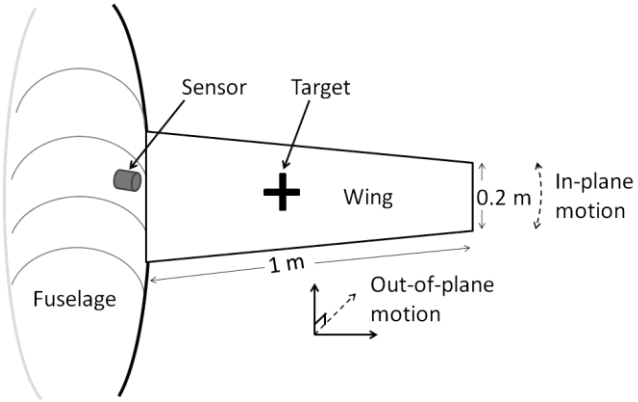

Fig. 11. Sensor-target arrangement on an aircraft.

modes and can then be related to the measured strains through the strain-displacement relationship. Most of the techniques developed in the literature used conventional strain gages, which need complex wiring in order to measure the strains at several points. Also, most of them can only detect static deformations or the deflections at a few interesting points of the moving structures. These indirect shape estimation techniques using strain measurements, which can come from foil gages and/or fiber optics Bragg gratings (FBG) become inefficient because of the weight of the gages, and costs associated with strain-displacement transformation. Besides these drawbacks, aircraft typically experience extreme temperature changes, which greatly affects the sensitivity of the strain gages. Also, the strain gauges require an external excitation source for their operation.

VI. Results

An experiment is devised using the testbed to simulate the motion of the wing of the small UAS described above. The wing is expected to bend less than 2.5 cm in the out-of-plane direction. The target used for this experiment is a 0.5 cm wide black vertical line that is 15 cm in length. Using the target control system, the target is oscillated horizontally across the field of view of the sensor. The sensor head is located 15 cm from the target in the orientation shown above in Fig. 6. In the actual application, the distance between the target and the sensor would be greater. For this experiment, we wanted to measure the sensor's response to a target travelling the entire distance between the centers of the two outside photoreceptor' FOVs, which is approximately 2.4 cm when the target is 15 cm from the sensor head. Figure 12 is an example of the data output from the sensor when the target is oscillating

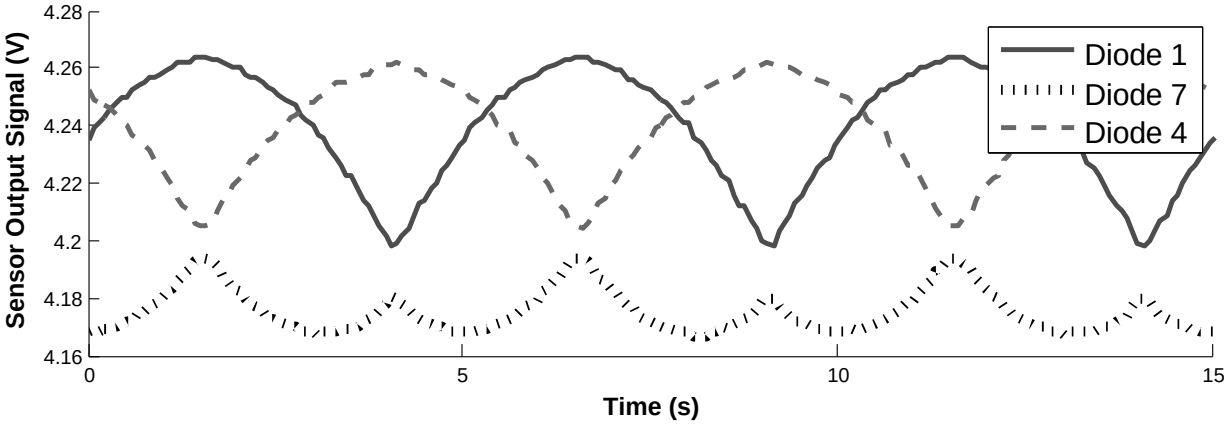

Fig. 12. Sensor output based on a 5 mm target moving 1.47 cm across the sensor FOV at 0.2 Hz.

across a distance of approximately 1.47 cm at 0.2 Hz.

For these results, the target is aligned so that it travels approximately between the centers of each of the two outside photoreceptors, D1. It can be deduced from the results shown in Fig. 12 that the target traveled closer to the center of the field of view of photoreceptor 1 than photoreceptor 4. This can be deduced by comparing the voltages from diode D1 and diode D4 at their minimum values. Throughout its travel, the target remains in the field of view of photoreceptor 7, resulting in troughs when it passes directly in the center of the field of view.

Comparing the signals from diodes 7 and 1, diodes 3 and 2, and diodes 4 and 7, linear regions are apparent between the troughs and peaks.

A target tracking algorithm utilizing the linear portions of these differencing signals, choosing which to use based on relative the position of the target, is able to produce a position value comparable to the actual position determined by a CCD camera. The results are shown in Fig. 14.

During the test, lasting 60 seconds, the compound eye sensor had an average error of 0.376 mm when compared with the target position as measured by the CCD camera. However, this error could be due in part to the 15 frames per second sampling rate of the CCD camera, which causes a delay in the target position calculation.

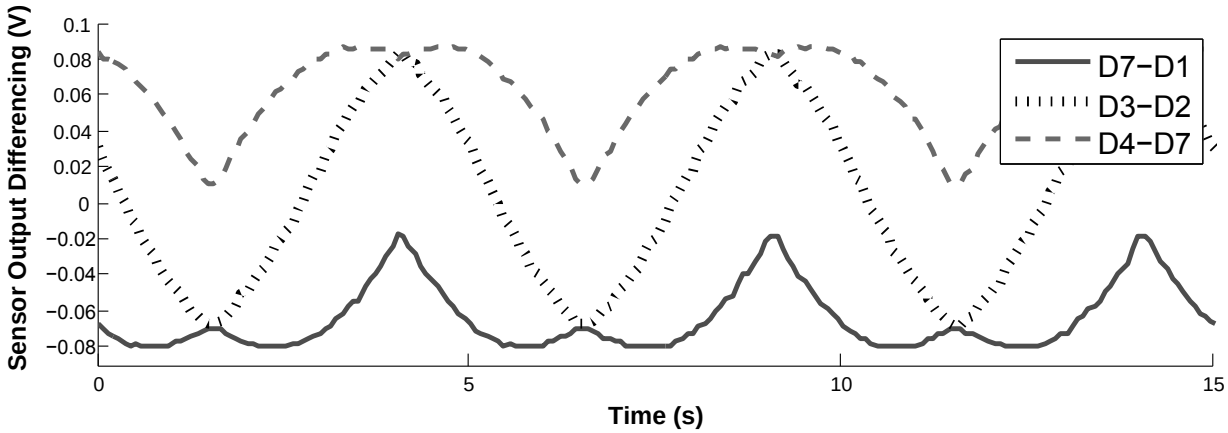

Fig. 13. Sensor output differencing based on a 5 mm target moving 1.47 cm across the sensor FOV at 0.2 Hz.

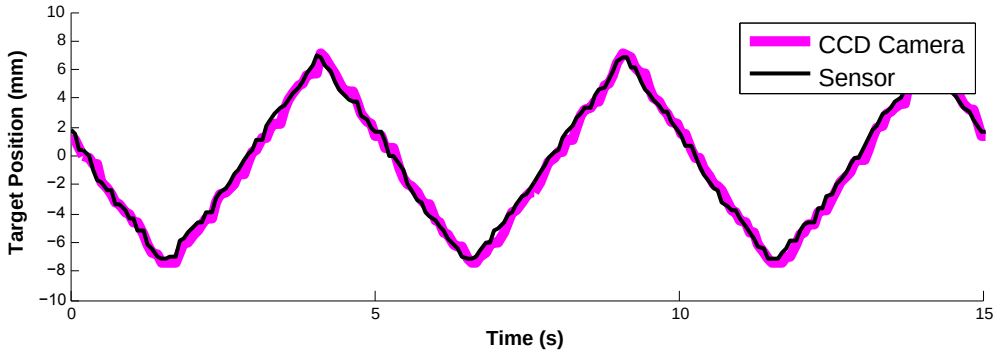

Fig. 14. Target position with time as determined by sensor and CCD camera tracking algorithms.

VII. Conclusions

This paper reports on efforts to develop a compound eye sensor to track a target for real-time measurement of wing deflection. The sensor has several advantages over conventional sensors used for this application, including lightweight, low power requirements, fast computation, and a small form factor. A new testbed for sensor characterization and target tracking algorithm development was described. The tests were run on this testbed allow the comparison of a standard CCD camera based target tracking algorithm with tracking algorithms based on the output of the compound eye sensor.

Acknowledgments

This work was performed with support from the NASA Aeronautics Research Institute.

References

[1] NASA Aeronautics Research Mission Directorate, [Online]. Available: http://www.aeronautics.nasa.gov/, Jan. 27, 2014.

[2] L. Librescu, and P. Marzocca, "Advances in the linear/nonlinear control of aeroelastic structural systems," *Acta Mechanica* 178.3-4 (2005): 147-186.

[3] M.J. Brenner, R.C. Lind, and D.F. Voracek. *Overview of recent flight flutter testing research at NASA Dryden*. Vol. 4792. National Aeronautics and Space Administration, Office of Management, Scientific and Technical Information Program, 1997.

[4] A. Derkevorkian, S. F. Masri, J. Alvarenga, H. Boussalis, J. Bakalyar, and W. L. Richards, "Strain-Based Deformation Shape-Estimation Algorithm for Control and Monitoring Applications", *AIAA Journal*, Vol. 51, No. 9 (2013), pp. 2231-2240, doi: 10.2514/1.J052215.

[5] P.M. Suh and D.N. Mavris, "Modal filtering for control of flexible aircraft", *Proceedings 54th AIAA/ASME Structures, Structural Dynamics, and Materials Conference*, Boston, MA, April 2013.

[6] P.M. Suh, A.W. Chin, and D.N. Mavris, "Virtual Deformation Control of the X-56A Model with Simulated Fiber Optic Sensors," *Proceedings AIAA Atmospheric, Flight Mechanics Conference*, Boston, MA, Aug. 2013.
[7] G. C. Holst, *Electro-Optical Imaging System Performance*, 3rd ed. SPIE Press, 2003.
[8] R. H. Vollmerhausen, D. A. Reago, Jr., and R. G. Driggers, *Analysis and Evaluation of Sampled Imaging Systems*, SPIE Press, 2010.
[9] B. Dean, "Light adaptation and applications for a fly eye vision sensor," Ph.D. dissertation, University of Wyoming, 2012.
[10] G. P. Luke, C. H. G. Wright, and S. F. Barrett, "A multiaperture bioinspired sensor with hyperacuity," *IEEE Sensors Journal*, vol. 12, no. 2, pp. 308–314, February 2012.
[11] R.W. Streeter, "Target tracking with a *Musca domestica* based sensor platform," M.S. thesis, University of Wyoming, 2013.
[12] Plastic Fiber Optic Photodarlington, Industrial Fiber Optics, Inc., 2006. [Online]. Available:http://www.fiberoptics.com/
[13] P. B. Bogert, E. Haugse, and R. E. Gehrki, "Structural shape identification from experimental strains using a modal transformation technique," *Proceedings 44th AIAA/AS-ME/ASCE/AHS/ASC Structures, Structural Dynamics, and Materials Conference*, 2003.
[14] G. C. Foss and E. D. Haugse, "Using modal test results to develop strain to displacement transformation," *IMAC*, vol. 1, pp. 112–118, 1995.
[15] A. Pisoni and C. Santolini, "Displacements in vibrating body by strain gauge measurements," *IMAC*, vol. 1, pp. 119–125, 1995.
[16] C. J. Li and A. G. Ulsoy, "High-precision measurement of tool-tip displacement using strain gauges in precision flexible line boring," *Mechanical Systems and Signal Processing*, vol. 13, pp. 531–546, 1999.
[17] P. B. Bogert, E. Haugse, and R. E. Gehrki, "Structural shape identification from experimental strains using a modal transformation technique," *Proceedings 44th AIAA/ASME/ASCE/AHS/ASC Structures, Structural Dynamics, and Materials Conference*, 2003.
[18] C. J. Li and A. G. Ulsoy, "High-precision measurement of tool-tip displacement using strain gauges in precision flexible line boring," *Mechanical Systems and Signal Processing*, vol. 13, pp. 531–546, 1999.